Mechanism for Burgess Shale-type preservation

Robert R. Gaines[a,1,2], Emma U. Hammarlund[b,c,d,1], Xianguang Hou[e], Changshi Qi[e], Sarah E. Gabbott[f], Yuanlong Zhao[g], Jin Peng[g], and Donald E. Canfield[b]

[a]Geology Department, Pomona College, Claremont, CA 91711; [b]Nordic Center for Earth Evolution, DK-5230 Odense M, Denmark; [c]Department of Palaeozoology, Swedish Museum of Natural History, SE-104 05 Stockholm, Sweden; [d]Department of Geosciences, Stockholm University, SE-106 91 Stockholm, Sweden; [e]Yunnan Key Laboratory for Palaeobiology, Yunnan University, Kunming 650091, China; [f]Department of Geology, University of Leicester, University Road, Leicester LE1 7RH, United Kingdom; and [g]College of Resources and Environment Engineering, Guizhou University, Guiyang 550003, China

Edited by Paul E. Olsen, Columbia University, Palisades, NY, and approved January 26, 2012 (received for review July 20, 2011)

Exceptionally preserved fossil biotas of the Burgess Shale and a handful of other similar Cambrian deposits provide rare but critical insights into the early diversification of animals. The extraordinary preservation of labile tissues in these geographically widespread but temporally restricted soft-bodied fossil assemblages has remained enigmatic since Walcott's initial discovery in 1909. Here, we demonstrate the mechanism of Burgess Shale-type preservation using sedimentologic and geochemical data from the Chengjiang, Burgess Shale, and five other principal Burgess Shale-type deposits. Sulfur isotope evidence from sedimentary pyrites reveals that the exquisite fossilization of organic remains as carbonaceous compressions resulted from early inhibition of microbial activity in the sediments by means of oxidant deprivation. Low sulfate concentrations in the global ocean and low-oxygen bottom water conditions at the sites of deposition resulted in reduced oxidant availability. Subsequently, rapid entombment of fossils in fine-grained sediments and early sealing of sediments by pervasive carbonate cements at bed tops restricted oxidant flux into the sediments. A permeability barrier, provided by bed-capping cements that were emplaced at the seafloor, is a feature that is shared among Burgess Shale-type deposits, and resulted from the unusually high alkalinity of Cambrian oceans. Thus, Burgess Shale-type preservation of soft-bodied fossil assemblages worldwide was promoted by unique aspects of early Paleozoic seawater chemistry that strongly impacted sediment diagenesis, providing a fundamentally unique record of the immediate aftermath of the "Cambrian explosion."

exceptional preservation | ocean chemistry | sedimentology

Burgess Shale-type (BST) fossil deposits are rare but occur globally in Early and Middle Cambrian strata (1, 2). Because they preserve the remains of soft-bodied organisms, which are typically absent from the fossil record, our understanding of the early evolution of the Metazoa is disproportionately based on these exquisite fossil biotas (3, 4). It has recently been demonstrated that a singular primary mode of preservation is shared among BST deposits worldwide. Soft-tissues, including cuticle, guts, eyes and gills are preserved as carbonaceous remains (3, 4) (Fig. 1), although mineralization of specific anatomical aspects (e.g., pyritization of limbs, ref. 5; phosphatization of guts, ref. 6) may occur in association. The preservation of organic tissues required protection of soft-bodied organisms from the processes that normally lead to their rapid degradation in sediments (7). Although anoxia in bottom waters is usually considered a prerequisite for BST preservation (8–10), anoxia alone cannot account for exceptional preservation because anaerobic degradation of labile tissues by sulfate reduction may proceed as rapidly as aerobic decomposition (11, 12). Although several hypotheses have been proposed to account for BST preservation (4, 9, 13), none have been previously tested, and the unusual abundance of exceptionally preserved biotas in the Cambrian (1) has not been adequately explained (14).

Here, we provide evidence from sedimentologic and sulfur isotope analyses, which indicate that the conservation of organic remains of fossils in the Burgess Shale, Chengjiang, and other BST deposits resulted from early inhibition of microbial activity in the sediments by means of oxidant deprivation. We demonstrate that this enigmatic taphonomic window resulted from the unique chemistry of the early Paleozoic ocean, which strongly influenced sediment diagenesis during the critical first few weeks after burial when soft tissues are typically lost to microbial degradation (15).

Entombment

Detailed petrographic analysis reveals that BST fossils occur exclusively within a diagnostic microfacies that is shared among all deposits. This microfacies is comprised of ultra-fine-grained claystones (all particles <25 μm) with pervasive early diagenetic carbonate cements (Fig. 2; see details in *SI Appendix*, Figs. S2–S4). Evidence for rapid entombment of soft-bodied fossils (16–18) within this facies is provided by randomly oriented clay microfabrics, indicating event-driven deposition of claystones from bottom-flowing density currents (19) (Fig. 2*A* and *SI Appendix*, Fig. S2) and by the chaotic orientations of soft-bodied fossils within individual claystone beds (20, 21). In most BST deposits, event-deposited claystone beds range from approximately 1 to 15 mm in thickness, but in the Chengjiang and Burgess Shale, event beds up to 8-cm thick are present (17, 18). In the Chengjiang, dark-colored claystones interpreted as hemipelagic deposits (18) occur between event beds, whereas at the Burgess Shale and other localities, event beds are stacked without intervening hemipelagic sedimentation.

Claystone beds are cemented by pervasive micron-sized authigenic calcium carbonates (9, 17), which are concentrated at bed tops and penetrate downward (Fig. 2 *B–E* and *SI Appendix*, Figs. S2–S4). Displasive growth of calcite rhombohedra within the claystone matrix (Fig. 2*C*) and the presence of bed top cements in *syn*-sedimentary slump features in the Walcott Quarry Member of the Burgess Shale and several other deposits, demonstrate that cements were emplaced near the sediment–water interface. The $\delta^{13}C$ of the carbonate cements from each of the deposits (*SI Appendix*, Fig. S5 and Table S2) lies largely within the ranges of late Early Cambrian and of Middle Cambrian seawater (22), indicating that cements were primarily derived from a seawater source, although a smaller contribution of organically derived bicarbonate to the cements from organic matter in the sediments is evident in some samples (23). These cements were likely important in preserving the primary, randomly oriented

Author contributions: R.R.G., E.U.H., and D.E.C. designed research; R.R.G., E.U.H., X.H., C.Q., S.E.G., Y.Z., J.P., and D.E.C. performed research; R.R.G., E.U.H., C.Q., S.E.G., Y.Z., J.P., and D.E.C. analyzed data; and R.R.G., E.U.H., X.H., C.Q., S.E.G., and D.E.C. wrote the paper.

The authors declare no conflict of interest.

This article is a PNAS Direct Submission.

Freely available online through the PNAS open access option.

See Commentary on page 5138.

[1]R.R.G. and E.U.H. contributed equally to this work.

[2]To whom correspondence should be addressed. E-mail: robert.gaines@pomona.edu.

This article contains supporting information online at www.pnas.org/lookup/suppl/doi:10.1073/pnas.1111784109/-/DCSupplemental.

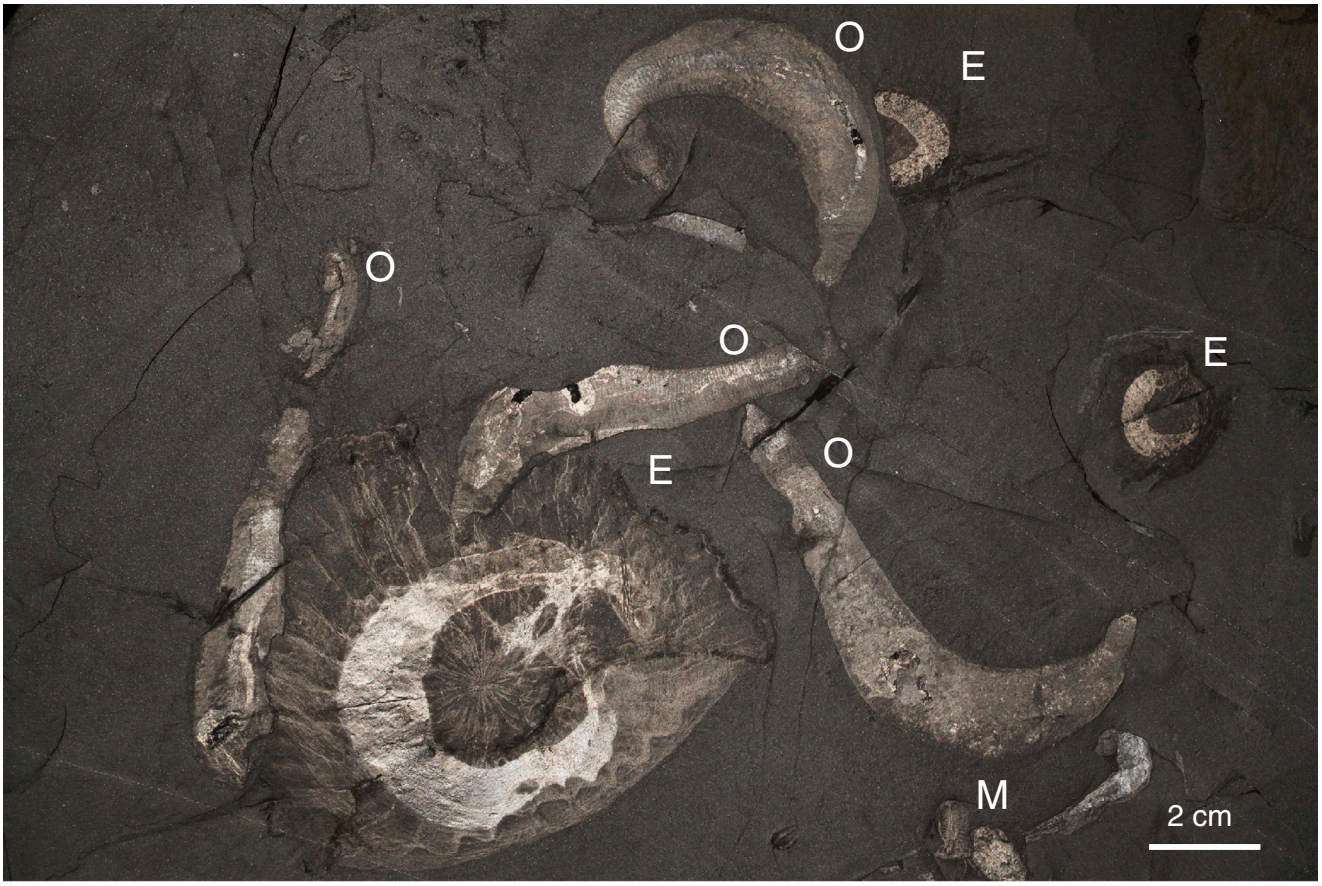

Fig. 1. Burgess Shale-type fossils from the Greater Phyllopod Bed of the Burgess Shale (Walcott Quarry Member), photograph taken in cross-polarized light. The fine details of soft-bodied anatomy are preserved as thin carbonaceous films. Soft-bodied fossils figured include examples of the priapulid worm *Ottoia prolifica* (O), the problematic medusiform animal *Eldoniia ludwigi* (E), and the arthropod *Marrella splendens* (M). Image courtesy of Jean-Bernard Caron (Royal Ontario Museum).

clay microfabrics which may be lost to compaction during burial. Direct precipitation of seafloor cements from seawater resulted from unusually high alkalinity of the Cambrian ocean (24, 25). In addition, carbonate precipitation may have been further influenced locally by flooding of bicarbonate-rich anoxic water masses onto the continents during transgressions (26) and by the high temperatures of epicratonic seaways lying at low latitudes (27).

Early Diagenesis: S_{PY} Isotopes.
The ubiquitous presence of bed-capping cements in BST bearing beds of all deposits analyzed suggests that they may have acted as a barrier, reducing porosity at the bed tops and restricting diffusion of oxidants into the sediments (9). We have tested this possibility using the isotopic composition of sulfur (δ^{34}S) in sedimentary pyrite (Fig. 2*F* and *SI Appendix*, Fig. S6 and Table S1). It is broadly accepted that BST deposits accumulated under anoxic or dysoxic bottom waters (4, 9, 12, 28), and as a result, SO_4^{2-} reduction was likely the primary pathway for degradation of organic remains (29). Analysis of 92 samples taken from a new drill core through the Chengjiang deposit shows systematic differences in δ^{34}S values between the fossil-bearing event layers and the finely interbedded background sediments (Fig. 3 and *SI Appendix*, Table S1). Background intervals are characterized by light δ^{34}S values (average $-6.0 \pm 0.6‰$) that display relatively high fractionations of 30–40‰ (30) from Cambrian seawater (*ca.* +30‰; ref. 31), indicating that microbial sulfate reduction was not impeded in these intervals (32). The great majority of the sediments in background intervals accumulated slowly by pelagic deposition (18), resulting in increased residence time of organic matter at or near the sediment–water interface. There, sulfate from the overlying seawater remained accessible to sulfate reducers, resulting in large δ^{34}S fractionations in these intervals. In contrast, the fossil-bearing event beds are characterized by heavy δ^{34}S values (average $+9.6 \pm 2.0‰$), with low fractionations. The average difference of 15.6‰ between the two closely interbedded lithofacies indicates SO_4^{2-} restriction in the porewaters of the claystone beds that preserve BST fossils (25). Event beds from the Burgess Shale ($n = 42$) are also characterized by similarly heavy δ^{34}S values (average $+22.6 \pm 0.6‰$), as are those of BST fossil-bearing intervals of the five other deposits analyzed (*SI Appendix*, Table S1; $n = 37$; average $+14.4 \pm 1.6‰$). Together, these data provide evidence of oxidant restriction within the BST microfacies in all deposits examined.

Rapid sediment deposition may result in enriched δ^{34}S values at the base of event beds when diffusion of SO_4^{2-} from overlying water is outpaced by SO_4^{2-} consumption within the sediments (33). We observe a general increase in δ^{34}S with depth within some event beds at Chengjiang, indicating some influence of burial on δ^{34}S. However, no down-bed trends are present in the Burgess Shale (*SI Appendix*, Fig. S6). In addition, δ^{34}S of event beds is not correlated with bed thickness (*SI Appendix*, Fig. S7), as would be expected if rapid deposition was the primary driver of SO_4^{2-} limitation within event beds. Furthermore, thin (millimeter) amalgamated event beds in the Burgess, Stephen, Kaili, Spence, Wheeler, and Marjum Formations contain similarly heavy δ^{34}S values that cannot be explained by the influence of event sedimentation alone because these beds were no more than 1- to 2-cm thick prior to compaction. Therefore, burial alone cannot

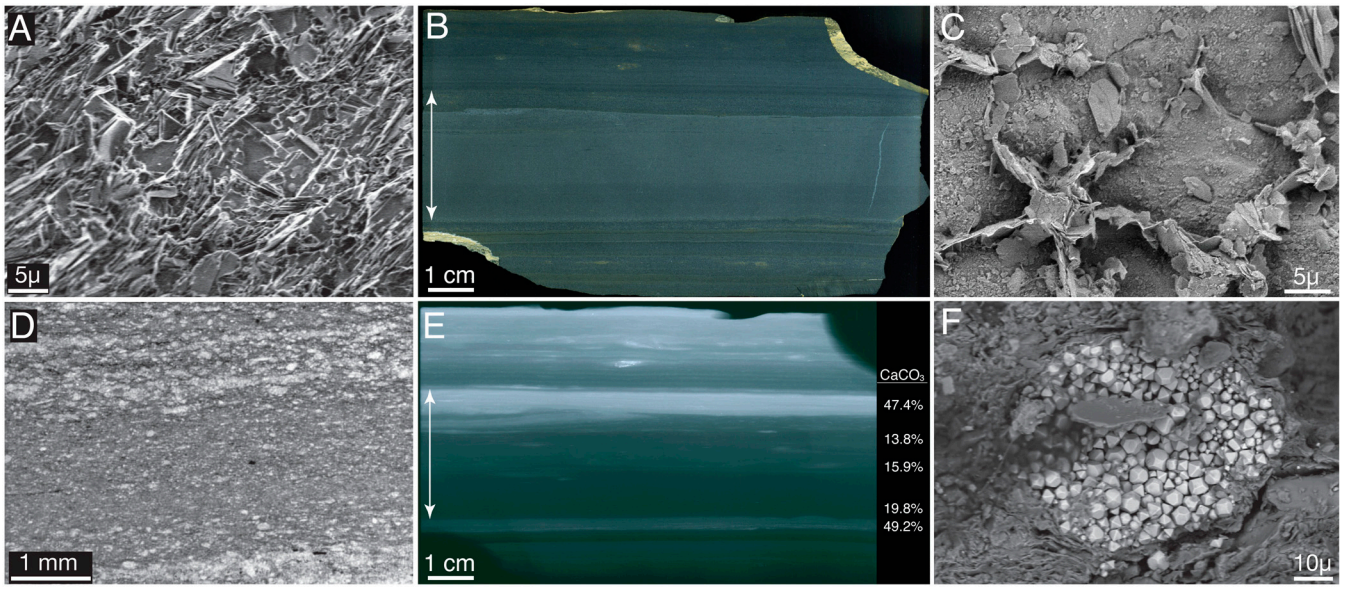

Fig. 2. Sedimentary and diagenetic fabrics of BST mudstones. (*A*) SEM micrograph of mudstone fabric in the "Great Eldoniia Layer" (GEL) of the Burgess Shale, showing random orientations of clay mineral grains and absence of coarser grained particles. (*B*) Polished slab showing the GEL (arrow) with thinner beds over and underlying it. (*C*) SEM micrograph showing displasive growth of 5–15 μ rhombohedra of authigenic calcite (low-lying areas) within an extensively cemented bed in the Wheeler Formation. Individual clay mineral grains have been forced to the margins of the calcite crystals. The sample has been etched with HCl; clays stand out in relief. (*D*) Thin section micrograph of Burgess Shale (Greater Phyllopod Bed) showing concentration of authigenic calcite cements (bright) at bed tops (at both the top and bottom of image). (*E*) X-radiograph of polished slab of Burgess Shale containing the GEL (arrow), showing the distribution of bed-capping authigenic carbonate cements. Bright areas correspond to high wt. % $CaCO_3$. Extensive bed-capping cement is present at the top of the GEL as well as at the tops of the thin, millimeter-scale beds that overlie it. (*F*) Backscatter SEM micrograph of pyrite cluster from a Chengjiang event bed at 12.96-m depth in the Haikou core showing fine grain size (1–5 μ) and aggregative habit of octahedra and pyritohedra.

account for the heavy $\delta^{34}S$ values that characterize BST microfacies of all deposits. Another mechanism of oxidant restriction is required.

Fossilization

BST preservation occurs only within a specific microfacies, indicating that specific qualities of the sediments were important in preservation. The sulfur isotope data, combined with low pyrite content (*SI Appendix*, Table S1) demonstrate that the mechanism of Burgess Shale-type preservation was oxidant restriction within porewaters, and that this restriction acted to severely slow the normal processes of microbial decomposition. The end result was incomplete degradation of organic remains and the conservation of soft-bodied fossils as carbonaceous compressions. Petrographic and geochemical data further suggest that pervasive, bed-capping authigenic carbonate cements, derived from a seawater source and emplaced near the sediment–water interface, acted as a permeability barrier at bed tops, restricting the flux of oxidants from overlying bottom waters into the sediments. The efficacy of this permeability barrier was greatly enhanced by the absence of bioturbation, a condition promoted by low concentrations of oxygen in bottom waters. Low oxygen acted to exclude a benthic fauna from the overwhelming majority of fossil-bearing intervals (13).

Experimental work has shown that soft-tissue decay is retarded in the absence of O_2 and SO_4^{2-} (12, 34). Hence, with oxygen-deficient conditions in the overlying bottom waters and burial in anoxic sediments (4, 9, 12, 28), microbial degradation of soft-tissues with O_2 was insignificant. Furthermore, $\delta^{34}S$ evidence indicates that sulfate concentrations within the sediments were sufficiently low to affect the rate and extent of microbial sulfate reduction (32). Sulfate reduction did occur, as evidenced by the presence of pyrite in beds bearing soft-bodied fossils (*SI Appendix*, Table S1). However, sulfate diffuses along a gradient, and although the flux of sulfate into the sediments was sufficient to generate the pyrite contents measured, sulfate concentrations in pore waters remained low enough to severely limit microbial activity (*SI Appendix*, Fig. S8).

After entombment in this microenvironment, degradation of soft tissues was sufficiently suppressed to allow the preservation of features of nonmineralized anatomy through a critical window in early diagenesis when labile tissues are typically lost (14). Soft-bodied fossils, which are preserved as two-dimensional carbonaceous films, have undergone considerable volume loss resulting from incomplete degradation of organic remains by limited sulfate reduction, as well as by fermentation, methanogenesis, and the action of autolytic enzymes (6). Limited degradation of soft tissues would have resulted in the collapse of organic remains (15), at which point the firm, ultra-fine-grained sediments played an important role in retaining the fine morphological detail of soft-bodied anatomy of fossils.

Ocean Chemistry and the Cambrian Taphonomic Window

Progressive oxidation of the early Phanerozoic ocean and its associated effects played an important role in the early evolution of the Metazoa (35–38), and our results suggest that ocean chemistry was also crucial in controlling the Cambrian taphonomic window for exceptional preservation (1). It is recognized that anoxic or dysoxic conditions were widespread in the global ocean (35, 37–39) and were present at the sites of deposition where BST preservation occurred (4, 9, 12, 28). A growing body of evidence also points to low-sulfate concentrations in Cambrian oceans relative to the modern (24, 39). Low-sulfate conditions are indicated by prominent global excursions in the isotopic composition of seawater sulfate (39) and by the presence of "superheavy" $\delta^{34}S$ of sedimentary pyrite in some settings (40). Low-sulfate conditions may have been promoted by the extensive burial of pyrite under widespread anoxic or dysoxic bottom waters (37) and by the lack of extensive bioturbation (41). Following the entombment of soft-bodied organisms in the early burial environment, elevated alkalinity of the Cambrian oceans (24, 25) promoted the emplacement of seafloor cements at bed tops.

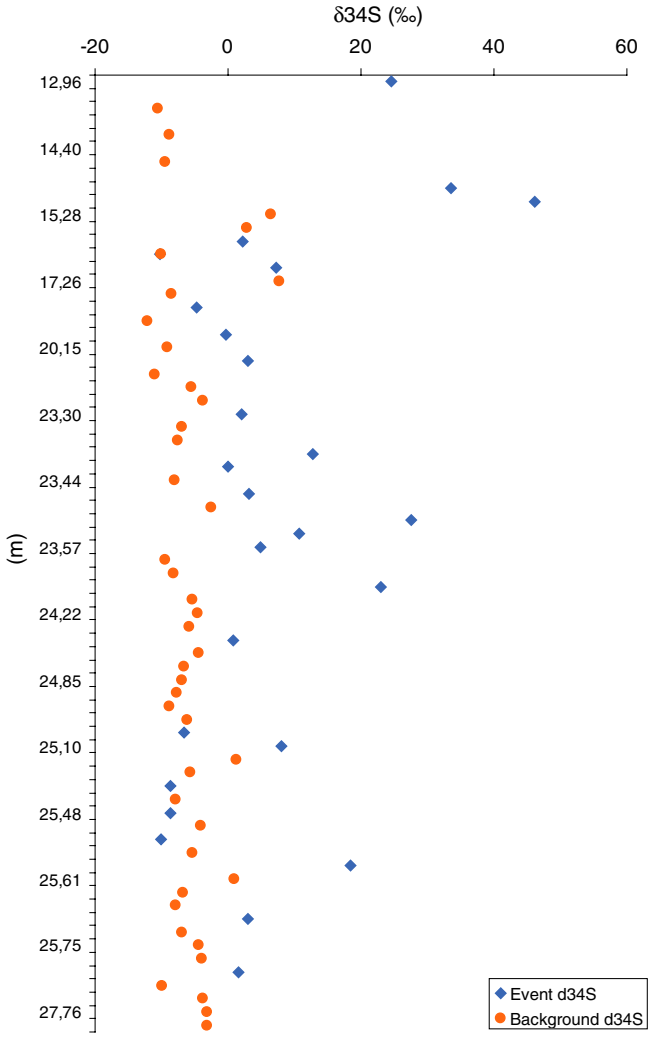

Fig. 3. Plot of the isotopic composition of the pyrite sulfur ($\delta^{34}S$) in the fossiliferous portion of the Chengjiang from a new drill core extracted near Haikou town, Kunming, Yunnan Province, China. Event-deposited beds (blue diamonds) are characterized by heavy values [average $+9.6 \pm 2.0‰$ (SEM)] that display less fractionation from Cambrian seawater (*ca.* +30‰; ref. 31) than background sediments [orange circles; average $-6.0‰ \pm 0.6‰$ (SEM)].

Sulfate limitation in the Cambrian oceans and widespread anoxic bottom water conditions provided a favorable starting condition for oxidant restriction in the sediments that was further exacerbated by the permeability barrier provided by bed-capping carbonate cements.

Conclusions

The widespread preservation of Burgess Shale-type assemblages of soft-bodied fossils during the Cambrian resulted from a combination of favorable sedimentary circumstances that acted to restrict the flow of oxidants into the early burial environment. Oxidant restriction was promoted by rapid entombment of soft-bodied organisms in sediments, followed by early cementation at the sediment–water interface, which resulted from enhanced alkalinity of Cambrian oceans. Low-SO_4^{2-} conditions in the global ocean and bottom waters locally depleted in O_2 further restricted the flux of oxidants required to sustain microbial activity in the sediments. Diffusion-limited conditions would have slowed the typical processes of microbial degradation in sediments by restricting the efficiency of sulfate reduction, thereby shifting the primary microbial pathways for degradation of labile carbon to the less efficient processes of methanogenesis and fermentation (11, 32). Together, these factors retarded the normal processes of microbial decomposition and facilitated the extraordinary preservation of soft-bodied fossil assemblages as carbonaceous films during this critical interval in the history of life.

Materials and Methods

Sample Localities. We described and systematically sampled a new core that penetrated the Chengjiang interval of the Early Cambrian (Series 2) Yu'anshan Formation at a soft-bodied fossil locality near Haikou, Yunnan. We also analyzed outcrop samples collected systematically from the Burgess Shale as well as a new BST locality in the upper Stephen Formation of the southern Canadian Rockies (42), the Spence Shale and the Wheeler and Marjum Formations of Utah, and the Kaili Formation of south China, all of Middle Cambrian age (Cambrian Series 3).

Chengjiang. A new core was drilled in July 2008 near Haikou town, Kunming, Yunnan province, China, one of the principal BST fossil-bearing localities, N24°46.535′ E102°34.160′.

Kaili Formation. Wuliu-Zengjayan section and Miaobanpo Quarry, Balang Village locality, Jianhe County, Guizhou, China (N 26°45.014′, E 108°24.982′).

Spence Shale Member of the Langston Formation. Miner's Hollow, Wellsville Mountains, Utah. Samples analyzed were collected from cycle 4 (N 41°35.744′; W 112°01.757′); Oneida Narrows locality, Franklin County, Idaho (N 42°19.271′; W 111°42.811′; ref. 43).

Burgess Shale Formation. Walcott Quarry Member, Walcott Quarry Locality, Yoho National Park, British Columbia, Canada (N 51°26′ 21.1″, W 116°28′ 19.1″); Raymond Quarry Member, Raymond Quarry locality, Yoho National Park, British Columbia (N 51°26′ 21.1″, W 116°28′19.1″); Campsite Cliff Shale Member, Mt. Stephen Trilobite Beds locality (N51°23′16.3″ W116°27′ 14.0″; ref. 44).

"Thin" Stephen Formation. Stanley Glacier locality, Kootenay National Park, British Columbia, Canada. Samples analyzed were collected from cycle 5 (N 51°10.781′, W 116°02.509′) (42).

Wheeler Formation. Wheeler Amphitheater locality, House Range, Millard County, Utah (N 39°21.874′, W 113°17.097′); Swasey Spring locality, House Range, Millard County, Utah (N 39°24.334′, W 113°15.699′); Drum Mountains locality, Juab County, Utah (N 39°30.249′, W 112°59.464) (10, 45, 46).

Marjum Formation. Marjum Pass locality, House Range, Millard County, Utah (N 39°14.798′, W 113°21.552′); Red Cliffs Wash Locality, House Range, Millard County (N 39°19′04.911″, W 113°16′19.988″); Sponge Gulch locality, House Range, Millard County, Utah (N 39°16′06.578″, W 113°18′33.393″); Pierson Cove Formation (lateral equivalent of Marjum Formation), Drum Mountains locality, Juab County, Utah (N 39°30.331′, W 112°159.736′) (10, 45, 47).

Petrologic and Compositional Analyses. Samples were collected in the field in the context of measured sections or drill core log. In the laboratory, samples were analyzed for physical and diagenetic fabrics using X-radiographs, thin sections, acetate peels, polished slabs, and scanning electron microscopy, using a LEO 982 Fe-SEM. SEM samples were prepared by breaking perpendicular to bedding, and were imaged using secondary electron and backscattered electron detectors at 5–15 kV. Elemental mapping of polished chips was conducted using a Bruker Energy Dispersive X-ray Spectrometer coupled to the Leo 982 Fe-SEM. Bulk rock mineralogy was determined by X-ray diffractometry of rock powders using a Rigaku Ultima IV diffractometer. Clay mineral separates were prepared using the method of Moore and Reynolds (48) and were analyzed using the same instrument. Weight percent carbonate was determined from rock powders by carbon coulometry using a UIC 5210 coulometer. Whole rock geochemistry was determined by X-ray fluorescence (XRF) analysis of fused glass beads analyzed with a Panalytical Axios XRF. All of the above analyses were conducted at Pomona College.

$\delta^{13}C$ and $\delta^{18}O$ Analysis of Carbonate. Whole rock powders were dissolved in phosphoric acid and the CO_2 evolved was analyzed online by mass spectrometry at Mountain Mass Spectrometry, the University of California, Davis Stable Isotope facility, and at the University of California, Riverside. Carbon

and oxygen isotopic compositions are expressed as permil (‰) deviations from Vienna Pee Dee belemnite using the conventional delta notation with a standard deviation no larger than 0.2‰ for both carbon and oxygen.

δ^{34}S Measurements of Pyrite. The δ^{34}S compositions of bulk rock samples were measured at the Nordic Center for Earth Evolution at the University of Southern Denmark. Rock samples were ground to a particle size below 63 μm and then distilled for inorganic sulfide with the Chromium Reducible Sulfur method (49, 50) and collected as Ag_2S. Selected thick event beds from the Haikou core (Chengjiang) and the Walcott Quarry Member of the Burgess Shale were subsampled across bedding and measured individually. Up to 300 μg of the Ag_2S precipitates were added to a tin cup with V_2O_5. Samples were combusted using a Thermo elemental analyzer coupled via a Conflow III interface to a Thermo Delta V Plus mass spectrometer. Sulfur isotope compositions are expressed as permil (‰) deviations from Vienna Canyon Diablo Troillite using the conventional delta notation with a standard deviation no larger than 0.2‰.

ACKNOWLEDGMENTS. We thank T. Abbott, P. Burke, F. Duan, Z. Feng, J. Tian, and X. Zhang for assistance in the field, and J. Caron, P. Fenton, D. Rudkin, and the Royal Ontario Museum for access to samples of the Burgess Shale and Stephen Formation (ROM-59951). Burgess Shale and Stephen Formation fieldwork was made possible by Parks Canada, especially H. Abbott, T. Kieth, A. Kolesch, M. Marpole, C. McClean, and J. Niddrie, D. Haley, R. Goossen, A. Lichtman, B. Markle, L. Schumacher, R. Stevens, D. Tanenbaum, C. Windham, and the staff at Nordic Center for Earth Evolution assisted with analyses. We thank M. Droser, S. Finnegan, N. Finke, N. Hughes, M. Kennedy, and M. Prokopenko for valuable discussions during the course of this work. We are grateful to T. Lyons and an anonymous reviewer whose comments improved the manuscript substantially. This work was supported by National Science Foundation EAR-1046233 and DMR-0618417, a D.L. and S.H. Hirsch Research Initiation Grant (R.R.G.), by the Swedish Research Council (E.U.H.), by the Danish Research Foundation (E.U.H. and D.E.C.), by the Royal Swedish Academy of Science (E.U.H.), and by the Natural Science Foundation of China 40730211 (to X.H.) and 40672018 (to Y.Z.).

1. Allison PA, Briggs DEG (1993) Exceptional fossil record: Distribution of soft-tissue preservation through the Phanerozoic. *Geology* 21:527–530.
2. Conway Morris S (1989) The persistence of Burgess Shale-type faunas: Implications for the evolution of deeper-water faunas. *Environments and Physiology of Fossil Organisms,*, , Transactions of the Royal Society of Edinburgh: Earth Science (Royal Soc Edinburgh, Edinburgh), Vol. 80, pp 271–283.
3. Gaines RR, Briggs DEG, Zhao YL (2008) Cambrian Burgess Shale-type deposits share a common mode of fossilization. *Geology* 36:755–758.
4. Butterfield NJ (1995) Secular distribution of Burgess-Shale-type preservation. *Lethaia* 28:1–13.
5. Gabbott SE, Hou XG, Norry MJ, Siveter DJ (2004) Preservation of Early Cambrian animals of the Chengjiang biota. *Geology* 32:901–904.
6. Butterfield NJ (2002) Leanchoilia guts and the interpretation of three-dimensional structures in Burgess Shale-type fossils. *Paleobiology* 28:155–171.
7. Froelich PN, et al. (1979) Early oxidation of organic matter in pelagic sediments of the eastern equatorial Atlantic: Suboxic diagenesis. *Geochim Cosmochim Acta* 43:1075–1090.
8. Butterfield NJ (1990) Organic preservation of non-mineralizing organisms and the taphonomy of the Burgess Shale. *Paleobiology* 16:272–286.
9. Gaines RR, Kennedy MJ, Droser ML (2005) A new hypothesis for organic preservation of Burgess Shale taxa in the middle Cambrian Wheeler Formation, House Range, Utah. *Palaeogeogr Palaeoclimatol Palaeoecol* 220:193–205.
10. Gaines RR, Droser ML (2010) The paleoredox setting of Burgess Shale-type deposits. *Palaeogeogr Palaeoclimatol Palaeoecol* 297:649–661.
11. Canfield DE (1994) Factors influencing organic carbon preservation in marine sediments. *Chem Geol* 114:315–329.
12. Allison PA (1988) The role of anoxia in the decay and mineralization of proteinaceous macro-fossils. *Paleobiology* 14:139–154.
13. Petrovich R (2001) Mechanisms of fossilization of the soft-bodied and lightly armored faunas of the Burgess Shale and of some other classical localities. *Am J Sci* 301:683–726.
14. Gaines RR, et al. (2012) Burgess Shale-type biotas were not entirely burrowed away. *Geology*, 10.1130/G32555.1.
15. Briggs DEG, Kear AJ (1994) Decay and mineralization of shrimps. *Palaios* 9:431–456.
16. Conway Morris S (1986) The community structure of the middle Cambrian phyllopod bed (Burgess shale). *Paleontology* 29:423–467.
17. Gabbott SE, Zalasiewicz J, Collins D (2008) Sedimentation of the Phyllopod Bed within the Cambrian Burgess Shale Formation of British Columbia. *J Geol Soc* 165:307–318.
18. Zhu M, Zhang JM, Li GX (2001) Sedimentary environments of the Early Cambrian Chengjiang Biota: Sedimentology of the Yu'anshan Formation in Chengjiang County, Eastern Yunnan. *Acta Paleontol Sin* 40:80–105.
19. O'Brien NR, Nakazawa K, Tokuhashi S (1980) Use of clay fabric to distinguish turbiditic and hemipelagic siltstones and silts. *Sedimentology* 27:47–61.
20. Whittington HB (1981) Rare arthropods from the Burgess Shale, Middle Camabrian, British Columbia. *Philos Trans R Soc B* 292(1060):329–357.
21. Zhang X-G, Hou X-G (2007) Gravitational constraints on the burial of Chengjiang fossils. *Palaios* 22:448–453.
22. Montanez IP, Osleger DA, Banner J, Mack LE, Musgrove M (2000) Evolution of the Sr and C isotope composition of Cambrian Oceans. *GSA Today* 10:1–7.
23. Kouchinsky A, et al. (2007) Carbon isotope stratigraphy of the Precambrian-Cambrian Sukharikha River section, northwestern Siberian platform. *Geol Mag* 144:609–618.
24. Brennan ST, Lowenstein TK, Horita J (2004) Seawater chemistry and the advent of biocalcification. *Geology* 32:473–476.
25. Peters SE, Gaines RR (2012) Formation of the Great Unconformity as a trigger for the Cambrian Explosion. *Nature*, in press.
26. Kempe S (1990) Alkalinity: The link between anaerobic basins and shallow water carbonates. *Naturwissenschaften* 77:426–427.
27. Landing E (2012) Time-specific black mudstones and global hyperwarming on the Cambrian-Ordovician slope and shelf of the Laurentia palaeocontinent. *Palaeogeogr Palaeoclimatol Palaeoecol*, 10.1016/j.palaeo.2011.09.005.
28. Allison PA, Brett CA (1995) In situ benthos and paleo-oxygenation in the Middle Cambrian Burgess Shale, British Columbia, Canada. *Geology* 23:1079–1082.
29. Jørgensen BB (1982) Mineralization of organic matter in the sea bed—the role of sulfate reduction. *Nature* 296:643–645.
30. Canfield DE (2001) Isotope fractionation by natural populations of sulfate-reducing bacteria. *Geochim Cosmochim Acta* 65:1117–1124.
31. Shields GA, Kimura H, Yang J, Gammon P (2004) Sulphur isotopic evolution of Neoproterozoic-Cambrian seawater: New francolite-bound sulphate d34S data and a critical appraisal of the existing record. *Chem Geol* 204:163–182.
32. Pallud C, Van Cappellen P (2006) Kinetics of microbial sulfate reduction in estuarine sediments. *Geochim Cosmochim Acta* 70:1148 1162.
33. Canfield DE, Raiswell R, Bottrell S (1992) The reactivity of sedimentary iron minarals toward sulfide. *Am J Sci* 292:659–683.
34. Hammarlund EU, et al. (2011) The influence of sulfate concentration on soft-tissue decay and preservation. *Palaeontogr Can* 31:141–156.
35. Canfield DE, et al. (2008) Ferruginous conditions dominated later Neoproterozoic deep water chemistry. *Science* 321:949–952.
36. Canfield DE, Poulton SW, Narbonne GM (2007) Late-Neoproterozoic deep-ocean oxygenation and the rise of animal life. *Science* 315(5808):92–95.
37. Dahl TW, et al. (2010) Devonian rise in atmospheric oxygen correlated to the radiations of terrestrial plants and large predatory fish. *Proc Natl Acad Sci USA* 107:17911–17915.
38. Dahl TW, et al. (2011) Molybdenum evidence for expansive sulfidic water masses in ~750 Ma oceans. *Earth Planet Sci Lett* 311:264–274.
39. Gill BC, et al. (2011) Geochemical evidence for widespread euxinia in the Later Cambrian ocean. *Nature* 469:80–83.
40. Ries JB, Fike DA, Pratt LM, Lyons TW, Grotzinger JP (2009) Superheavy pyrite (delta(34) S(pyr) >delta(34)S(CAS)) in the terminal Proterozoic Nama Group, southern Namibia: A consequence of low seawater sulfate at the dawn of animal life. *Geology* 37:743–746.
41. Canfield DE, Farquhar J (2009) Animal evolution, bioturbation, and the sulfate concentration of the oceans. *Proc Natl Acad Sci USA* 106:8123–8127.
42. Caron J-B, Gaines RR, Mángano MG, Streng M, Daley AC (2010) A new Burgess Shale-type assemblage from the "thin" Stephen Formation of the southern Canadian Rockies. *Geology* 38:811–814.
43. Liddell WD, Wright SH, Brett CE (1997) Sequence stratigraphy and paleoecology of the Middle Cambrian Spence Shale in northern Utah and southern Idaho. *Brigham Young Univ Geol Stud* 42:59–78.
44. Fletcher TP, Collins DH (1998) The Middle Cambrian Burgess Shale and its relationship to the Stephen Formation in the southern Canadian Rocky Mountains. *Can J Earth Sci* 35:413–436.
45. Robison RA (1991) *Middle Cambrian Biotic Diversity; Examples from Four Utah Lagerstätten* (Cambridge Univ Press, Cambridge), pp 77–93.
46. Brett CE, Allison PA, DeSantis MK, Liddell WD, Kramer A (2009) Sequence stratigraphy, cyclic facies, and lagerstätten in the Middle Cambrian Wheeler and Marjum Formations, Great Basin, Utah. *Palaeogeogr Palaeoclimatol Palaeoecol* 277:9–33.
47. Rigby JK (1983) Sponges of the Middle Cambrian Marjum Limestone from the House Range and Drum Mountains of Western Millard County, Utah. *J Paleontol* 57:240–270.
48. Moore DM, Reynolds RC (1997) *X-ray Diffraction and the Analysis of Clay Minerals* (Oxford Univ Press, Oxford), pp 179–201.
49. Lyons TW (1997) Sulfur isotopic trends and pathways of iron sulfide formation in upper Holocene sediments of the anoxic Black Sea. *Geochim Cosmochim Acta* 61:3367–3382.
50. Newton RJ, Bottrell SH, Dean SP, Hatfield D, Raiswell R (1995) An evaluation of the use of the chromous chloride reduction technique for isotopic analysis of pyrite in rocks and sediments. *Chem Geol* 125:317–320.